Image analysis assessment of the effect on mixing on aqueous dissolution of CO2 and air bubble swarms in a bubble column

Legendre Suarez, Daniel; Zevenhoven, Ron

Published in:
Chemical Engineering Research and Design

DOI:
10.1016/j.cherd.2019.04.008

Published: 01/01/2019

Document Version
Accepted author manuscript

Accepted Manuscript

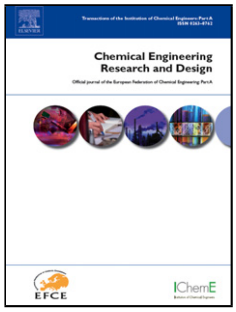

Title: Image analysis assessment of the effect on mixing on aqueous dissolution of CO_2 and air bubble swarms in a bubble column

Authors: Daniel Legendre, Ron Zevenhoven

PII: S0263-8762(19)30163-7
DOI: https://doi.org/10.1016/j.cherd.2019.04.008
Reference: CHERD 3604

To appear in:

Received date: 11 October 2018
Revised date: 3 April 2019
Accepted date: 5 April 2019

Please cite this article as: Legendre D, Zevenhoven R, Image analysis assessment of the effect on mixing on aqueous dissolution of CO_2 and air bubble swarms in a bubble column, *Chemical Engineering Research and Design* (2019), https://doi.org/10.1016/j.cherd.2019.04.008

Revised manuscript for Chemical Engineering Research and Design (CHERD)

Image analysis assessment of the effect on mixing on aqueous dissolution of CO_2 and air bubble swarms in a bubble column

Daniel Legendre[a] and Ron Zevenhoven[a*]

[a] *Thermal and Flow Engineering Laboratory, Åbo Akademi University, FI20500 Turku, Finland.*

**corresponding author: ron.zevenhoven@abo.fi*

Graphical abstract

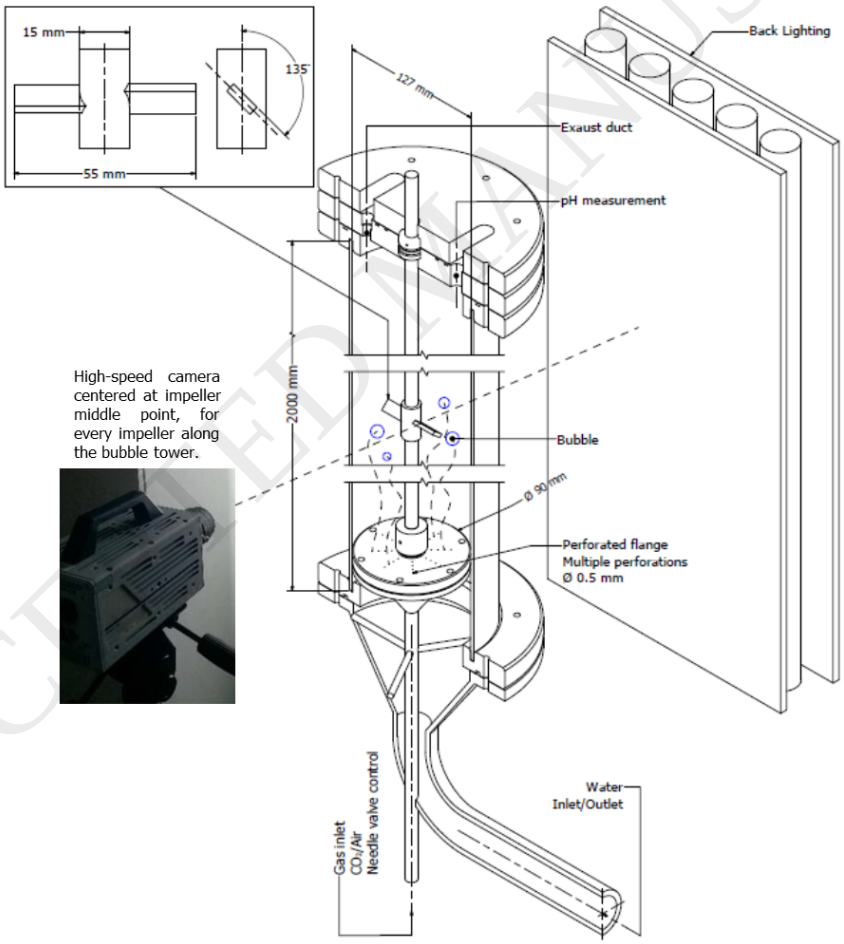

Semi-cross section of the bubble reactor with high-speed camera placement and back lighting.

Highlights

- Bubble swarm dissolution is studied experimentally using a high speed camera
- Clearly different bubble size distributions for CO_2 and non-dissolving air bubbles
- While dissolving, bubble size distribution narrows and bubble sphericity increases
- An increase in impeller rotation speed enhances bubble swarm dissolution.
- Comparison with boundary layer dissolution models shows small deviations.

Abstract

Many processes for capture and use of carbon dioxide, CO_2, involve aqueous solutions containing salts, the dissolution of CO_2 being rate-determining. For bubble column reactors, mixing the solution may increase the dissolution rate, reducing the necessary height. For this paper, extending an experimental cylindrical bubble tower set-up by the inclusion of mixers enables to observe the performance of multiphase bubble reactors. These experiments were done to gain deeper understanding on the dissolution and later chemical conversion of CO_2 bubble swarms in agitated vessels. Bubble swarms of ~100 bubbles were tracked using a high-speed camera. Comparison of the dissolution rate of bubble size distributions at different heights in a 2 m column revealed significant rates of CO_2 mass transfer in contrast with hardly any change in the bubble size distribution for air. Results are consistent with the dissolution of single rising bubbles, and previous one-way coupling simulation shows a fair agreement with the experimental results. CO_2 bubbles showed a smaller average size while increasing their bubble sphericity as function of height in the column. Initially, bigger CO_2 bubbles present a wobbly behavior and trajectories, becoming more spherical while dissolving. The effect of the stirred environment increases as bubbles dissolve, affecting trajectories and velocities, as smaller spherical bubbles don't show a linear rising trajectory. Comparing results without and with mixing showed that increased mixing rates bring down the height needed for dissolution, especially in the middle section of the column, where bubbles are no longer wobbly yet are not yet very small.

Keywords: CO_2, air, bubble swarm dissolution tracking, bubble tower, mixing environment, image analysis

1 Introduction

The endeavor to produce a theoretical description of bubble cluster dissolution in fluids where the transferred material reacts with species dissolved in the liquid phase is a compelling engineering development that could result in simplifications of upstream or downstream processing. This would make it possible to give design values, for a certain gas/liquid combination, for the maximum gas flow or minimum reactor height that would produce complete dissolution including total chemical conversion of a gas phase into a liquid phase

(Legendre and Zevenhoven, 2016). Reactor design parameters can target circumstances where no gaseous products are generated and hence no outlet needed.

It is estimated that 25% of all reactions in this industry take place in multiphase liquid-gas flows (Martín et al., 2011). Despite all this, even after significant modelling efforts at academia (Gong et al., 2007; Huang et al., 2018; Wang et al., 2018; Zhang et al., 2018) bubble reactor engineering for example for scale-up of the Slag2PCC process is closer to an art than a science, using low-accuracy algorithms that disturb the physics reflected by the models implemented (Jakobsen, 2001). Therefore, it may not be appropriate to actually explain the dissolution of a bubble swarm in a chemical reactor by the studying a single isolated bubble. Nonetheless, (Colombet et al., 2015) recently reported (for O_2 bubbles dissolution in water) that the Sherwood number quantifying the mass transfer for single rising bubbles is close to that for swarms for a given Reynolds number based on average vertical bubble rise velocity. This was found to hold for gas volume fractions up to 30%, for slow diffusion of the gas in the liquid (i.e. a high Péclet number). Moreover, it is stated that mass transfer conditions are similar to those for a bubble rising in a fluid at rest. The results given here allow for analysing this for CO_2: Péclet numbers cannot be large for very small bubbles of a gas with a higher solubility in water than oxygen. Additional physical phenomena are added by the turbulent mixing environment of the system and interactions between bubbles occur even at small gas volume fractions.

One important liquid-gas flow is encountered in the so called Slag2PCC process (Mattila and Zevenhoven, 2014) designed and being scaled up at Aalto University in cooperation with Åbo Akademi University in Finland. This is seen as one of the portfolio of efforts in the field of carbon capture, utilization and storage (CCUS), aiming at valorization of calcium-based industrial wastes (here: steelmaking slag) using carbon dioxide, producing precipitated calcium carbonate (PCC) with significant market value. The rate-determining step of this carbonation process is the dissolution of CO_2 bubbles, since ideally only negligible amounts of it leave the process with exhaust gases. Mixers such as those used in the carbonation reactor (as well as in the upstream reactor for calcium extraction, using ammonium salt solvent) to further improve solution mixing, can be put into the here used bubble tower reactor as well, similar to the Slag2PCC carbonation reactor as part of the demonstration-scale process unit at Aalto University (Said et al., 2016). For the purpose of the present work only CO_2 or air dissolution in water is studied.

A more detailed experimental procedure applied to actual operating conditions of a chemical reactor may give the information necessary to expand and improve models on CO_2 dissolution that would allow for increasing the dissolution rate of gases in liquids. Previous estimations using computational fluid dynamics (CFD) Euler-Lagrange one-way coupling calculations (Legendre and Zevenhoven, 2016) on CO_2 bubble swarm dissolution (with initial bubble diameter D_{Bubble}=5 mm) at low gas volume fraction gave an estimated 1.95 m height in the vessel to be sufficient to reach total bubble (swarm) dissolution in water at ambient conditions. These numerical estimations show the need to modify the original design of the Slag2PCC carbonation process step, suggesting that a new reactor tank of a similar height is required, depending on the intensity of mixing used. The forces applied by an impeller to the material contained in a vessel produce a characteristic flow pattern that depends on the impeller geometry, properties of the fluid, and the relative sizes and proportions of the tank, baffles and impeller (Cheremisinoff, 2000). This can nowadays be simulated with reasonably accuracy

using CFD. In a chemical reactor the dissolution of a gas stream into fluid phase is one of the most recurrent phenomena in the chemical industry, which may be driven by pure diffusion, convection or chemical reaction effects. Diverse state-of-the-art models aim at predicting a certain dissolution rate, but still validation of numerical models is needed (Joshi, 2001).

We recently (Leendre and Zevenhoven, 2016) presented a 3D one-way coupling method to simulate the dissolution of a number of small CO_2 bubbles in a bubble reactor with mixing impellers. The aim of the experimental results in this paper is to give a quantitative estimation of CO_2 bubble swarm dissolution. Here, a bubble swarm is defined as a dense group of (rising) bubbles, particularly for the current research in a chemical reactor with mixers. Thus, experimental results presented in this paper can be used as a starting point for improving numerical models involving large numbers of rising bubbles.

1.1 Reflections on earlier work by others

A literature review of different experimental approaches for single bubble rising, based on different techniques on different tank cross sections (cylindrical and rectangular) was recently given by (Böhm et al., 2014). Furthermore, a statistical tool with image analysis on free rising bubble swarms in a rectangular column with discriminant factorial analysis was developed by (Ferreira et al., 2012), successfully measuring the bubble size distribution (BSD) of a swarm and being able to distinguish three classes different classes of bubbles due to overlapping: single bubbles, medium complexity bubbles and large complexity bubbles, respectively (See Fig. 5 of (Ferreira et al., 2012)).

The current research involves only small gas area fractions <7%, therefore as bubbles that are scattered across the pipe which are all treated as single bubbles, as medium complexity bubbles are rare and are rapidly dispersed by the impeller rotation. Moreover, errors derived from overlapping should be suppressed by statistical means given that a large bubble sample is used. In the present experimental case, samples of 100 000 entities tracked are used to measure the sizes of a swarm of ~100 bubbles in a 1 second recording video. Furthermore, in the case of larger gas fractions, bubbles overlapping becomes an issue, and diverse algorithms to study dense bubble swarms can be used to study highly overlapping bubbles. For example through calculating the overall perimeter of a segment and then find the points on the perimeter that represent the connecting points of overlapping objects and from that cluster perimeter arcs that belong to the same object to fit ellipses on the clustered arcs of the perimeter (Honkanen et al., 2005). Another suitable manner to address overlapping bubbles was developed by (Zhong et al., 2016), who proposed a method that involves the use of a template database for deformed bubbles, splitting contours for every overlapped single bubble in a bubble swarm giving a the data base for use as a template for recognition of similar shapes for further contour split.

An important study focusing on the calculation of bubble size distributions using statistical methods and supported by the aspect ratio obtained by image analysis with optical probe measurements was made by (Besagni et al., 2016), who used an experimental facility consisting of a vertical pipe of Plexiglas of diameter = 0.24m, height = 5m and a six arm spider sparger with holes as gas inlet. This dense two phase (air-water) bubble column flow does not include mixers. In this investigation major emphasis was put on the estimation of BSD as a means to

understand the dynamics that rule this system. Further investigation with this facility was made (Besagni and Inzoli, 2016) and optical probe measurements at different axial and radial positions were reported for air-water systems. The evolution of the equivalent diameter distribution at different heights of the reactor in the sparger region was reported, showing changes on relative frequency of diameter intervals. As their study involves counter- current dense air-water bubble columns the nucleating bubbles, channeling, clustering/coalescence and segregation of agglomerates all affect the BSD of the system. Moreover, that work is centered on flow regimes transition and BSD changes due to local flow properties, with no mention of gas dissolution in the fluid phase. Nevertheless, their investigation provides a large data set to validate numerical methods.

A study on agitated vessels was made by (Laakkonen et al., 2005), measuring local BSD in a Rushton turbine agitated 14 dm^3 vessel with air-deionized water and CO_2-n-butanol. Deliberately those gas-fluid combinations were chosen as the dissolution of the gas phase into the liquid phase is low, therefore no perceptible, .and no mention is made of dissolution as a mechanism that affects the BSD. With a fully baffled glass vessel of 260 mm height and an impeller rotating speed of 260-490 rpm, three experimental techniques were evaluated: Capillarity suction probe (CSP), Phase Doppler Anemometry (PDA) and Digital imaging (DI), respectively. Even though some deviations were found, mostly due the size range for each technique, CSP and DI showed good agreement and successfully measured the BSD in Point wise BSD and spatially average BSD for each technique respectively. Furthermore, only DI can estimate bubble shapes although some bias exists in image analysis techniques due to edge detection and depth of field errors.

2 Experimental set up and instrumentation

Previous experimental results determined by means of image processing (Legendre and Zevenhoven, 2017), showed the almost complete dissolution of 5 mm free rising CO_2 bubbles within a 2 m high, 12.7 cm inner diameter polycarbonate bubble column. Bubble initial size was found to be stable and approx. 5 mm for CO_2 with a 0.5 mm centered orifice feeding flange. For the current paper, four pitched blade impellers were added to the bubble column. Impellers are located in the middle point of four 48 cm dividing sections, as the gas distributor in the reactor is elevated 8 cm for construction/maintenance reasons. This gas distributor, shown in more detail, has eight lines of four holes (0.5 mm) at 45° angles between the lines of holes (Fig. 1).

A further expansion on the method for the tracking of a single rising bubble was made to study the dissolution dynamics of a continuously fed bubble CO_2 swarm in a stirred environment, as a means to assessment of the dissolution process on the Slag2PCC process, aiming at studying the effect of mixing in the rate of dissolution. The image recording set-up consisted of a high-speed Photron camera SA3 Model 120K-M3 equipped with a 52 mm Nikon 200773 lens. To avoid reflections and shadows the lighting, supplied by a set of parallel arrangement of fluorescence tubes T5 39 W was put behind the column. Videos of 1 s duration were taken at different heights: both the camera and the lighting vertical position could be adjusted. Video

recordings were taken around the mixing impellers and at the height of the gas inlet. The distance from the camera (lens) to the column was ±45 cm while the lighting was ±20 cm behind the column. This gave a window of ~14.5 cm used for all measurement heights (Fig. 2). The resolution of the recording is 6.9 pixel/mm at a frame rate of 1000 images per second with a constant exposure of 1/2000.

Pure CO_2 or air was fed from a bottle equipped with a rotameter flow meter calibrated for air and CO_2 allowing for flows up to 0.9 and 0.5 l /min (STP), respectively. All tests reported here were done at ambient conditions, with temperatures in the range 18.3 - 22.4 °C, with a gas flow of 0.25 l / min STP. The column solution was flushed and new (tap) water was taken when the solution pH, measured at the top of the column, dropped to values below 5.7, thus assuring <5% saturation of water with CO_2. (High levels of saturation will eventually slow down CO_2 dissolution.) Impeller rotational speed was 0, 50, 100, 150 or 200 rpm. Spatially average BSDs for each impeller section are reported.

3 Quantitative image processing and bubble swarm analysis (high-speed camera tracking)

3.1 Image processing

Tracking bubble sizes, shapes and velocities of bubble swarms in an aqueous solution mixed with rotating impeller using image recording and analysis is not a straightforward procedure, hence it is tackled in different steps addressing each challenge for accurate bubble recognition and quantification. This is due to the complex behavior of the bubble swarm in a mixed fluid environment, plus the effect of optical distortion due to the curvature of the vessel and the fluid surrounding the gas phase. Several processing steps are needed to make the images suitable for for bubble swarm analysis, which can be listed as:

1. Background synchronization
2. Optics distortion correction
3. Filtering and contrast enhancement
4. Level setting for black and white conversion

Details and images that illustrate this procedure are given in the Supplementary Material.

3.2 Bubble size and shape estimation

The recorded images are processed using the Matlab® image processing toolbox concatenated to the previous processing steps to extend the earlier capabilities of single bubble tracking (Legendre and Zevenhoven, 2017) to multiple bubble swarm tracking. Several authors have used this shadowgraphy technique (Nock et al., 2016) (Colombet et al., 2011), with acceptable results, as the technique is generally standard. For the present paper after the four pre-processing steps mentioned above this routine is based on:

i. the removal of the background detail,
ii. threshold iteration for black and white (B & W) conversion,
iii. size position filtering,
iv. edge detection and filling of structures,
v. size, shape and position estimation in base of a reference point and finally
vi. ellipse fit.

The overall procedure can be grouped as three steps as shown in (Fig. 3).

Some bubble overlapping occurs, as seen in Fig. 3, nevertheless due to low gas area fractions these bubbles are located at relative separate planes (distance between planes >> bubble diameter), and due to the impeller rotational motion these bubbles move at different speeds. Therefore, the overlapping of two bubbles in a frame is rapidity scattered in the subsequent frames of motion. This statement is further corroborated below in Fig. 5, where it can be appreciated that apparently large bubbles from bubble cluster overlapping (bubble diameter >7-8 mm), present a low frequency of appearance (number of bubbles < 5) in the recorded 1000 frames videos, even if locally in a single frame a large number of overlapping bubble clusters can be seen in Fig. 3.

Following a similar path as (Colombet et al., 2015), all bubbles here are assumed to be oblate spheroids with a minor semi-axis "*a*" and a major semi -axis "*b*", while the third semi axis "*c*" is assumed to be equal to the major semi axis "*b*", measured from the two dimensional parameters of the ellipse fit, using the bubble aspect ratio $\chi = b/a$. The estimated bubble diameter is then estimated from the volume of this spheroid as:

$$d = (8b^2a)^{\frac{1}{3}} \qquad \textit{(Eq.1)}$$

The Void Area fraction (gas fraction) is calculated as the ratio of pixels recognized as bubble ($Pixel_{Bubble}$) and the pixels recognized as background ($Pixel_{Background}$):

$$VoidAreafraction = \frac{Pixel_{Bubble}}{Pixel_{Background}} \text{ x } 100\ [\%] \qquad \textit{(Eq.2)}$$

3.2.1 Sauter mean diameter (d_{32})

The Sauter diameter (d_{32}) is a volume/surface area ratio diameter, commonly used for rate and efficiency studies in mass transfer and reaction applications (Azzopardi, 2011). This is better suitable to evaluate dissolution of bubble swarms where the dissolution is followed by a chemical reaction close to the surface of the bubble.

All bubbles are treated as ellipsoids, therefore the volume of each bubble is defined as:

$$Volume_{Bubble} = \frac{4}{3}\pi abc \qquad \textit{(Eq.3)}$$

As the bubbles are assumed to be oblate spheroids; their superficial area is defined using a derivative approximation formula (Klamkin, 1971) (Eq. 4), that depends on a bounded exponent 1< p < 2. A furthermore approximation for p = 1.6075 yields an error <1.42%, known as the Knud Thomsen equation (Michon, 2000).

$$A_{SuperficialBubble} = 2\pi(a^p b^p + a^p c^p + b^p c^p)^{\frac{1}{p}} \qquad (Eq.4)$$

Finally, when the actual surface area of the bubbles and their volumes are known the Sauter diameter can be expressed as:

$$d_{32} = 6\frac{Volume_{Bubble}}{A_{SuperficialBubble}} \qquad (Eq.5)$$

4 Results

Images from video recordings in a bubble tower are analyzed with the objective to obtain a quantitative estimation of the bubble swarm dissolution phenomena. This is done in terms of the position inside the reactor and rotational speed of the impellers used. This quantitative estimation is based on the estimation of bubble size distribution evolution in four reactor sections.

All images are processed using a level set selection for black and white conversion algorithm as described in the Supplementary Material "S4 Level set for black and white conversion". This algorithm should in principle via statistical means and Pareto front optimization ensure that noise is deleted from the videos, avoiding that noise is tracked as a very small bubble. Furthermore, all videos have a high pass filter for the minimum bubble diameter size, for practical purposes this value is selected to be 0.5 mm i.e. approx. 3.5 pixels. For the extreme case of a bubble diameter equal to 3 pixels, the maximum overestimate area error is 29 %; this error becomes smaller as the bubble size increases due to a more pixel resolution used to measure the bubble area.

4.1 Effect of vertical position

Dissolution of bubbles cannot truly be appreciated in Fig. 4 for air bubbles as the mean diameter of the bubble swarm oscillated between 3.70 and 4.51 mm, furthermore no clear variation can be appreciated in the shape of the bubble size distribution between impellers (column sections) 1-4. This in contrast with a clear dissolution of CO_2 bubbles in Fig. 5 as the bubbles ascend by number of impeller from 3.90 mm to 1.50 mm in the highest section of the tower, with a clear shift of the BSD towards tsmaller diameters as the bubbles ascend. All diameters intervals are reported with their respective standard deviation as the average of 1000 images/s.

4.1.1 Bubble shape

In Fig. 6.a as expected air bubbles of the current sizes present a spreaded aspect ratio $\chi \in$ [1-6] with a similar number of bubbles with χ < 3, although a mild tendency of air bubbles to become more spherical while rising is found. All χ distribution partitions preserve the same order of magnitude irrespective of impellers location. In contrast Fig. 6.b reflects the aspect ratio distribution for CO_2 bubbles, where it can be seen that the number of bubbles in the smallest

i.e. more spherical aspect ratio range $\chi \in [1\text{-}1.25]$ (see Fig.12 in (Legendre and Zevenhoven, 2017)) increases drastically from approx. 10 bubbles in the lowest tower section to almost 120 entities around the highest impeller. A clear shift of the original χ distribution towards the more spherical bubbles $\chi \sim 1$ is appreciated as CO_2 bubbles rise and dissolve. It is also noted that the number of bubbles in every impeller frame increases from ≈ 83 to ≈ 140 as the bubbles dissolve. This must be a result of a combined effect that smaller bubbles have less tendency of being overlapped in the same image and that smaller bubbles are rising slower; therefore bigger bubbles from lower heights catch up with small ones as they ascend.

4.1.2 Gas area fraction

The variable void area fraction defined in Eq. 2. that represents the gas area fraction of CO_2 or air is used to motivate the use of a 1 second recording from a video analyzed. Since the experimental procedure was designed to perform under steady state conditions with a constant gas flow of 0.25 l/min (STP) and further constant values of gas area fractions measured for each video as presented in Fig. 7, it can be concluded that there have not been significant not large variations in the gas-liquid system presented in the current research.

In terms of gas void area fraction in Fig 7.a for air bubbles, it is seen to oscillate in the range 3 - 6.5 %, even when the fraction for the first section seems higher than for other sections. Eventually it stabilizes and reaches values around 4 – 5 % towards the end of the graph. For the CO_2 counterpart in Fig 7.b it can be observed that the first impeller section presents the highest void area fraction 4% but after this, towards the impellers 2-3-4 higher up this void fraction levels out at around 2%.

In terms of oscillations of this variable in Fig. 7, a full cycle of oscillation is captured within 1 second images recording of the system. Even in the worse configuration of Fig. 7 for for example "b" impeller 1, the void fraction fluctuates between 3.5 % and 5 %. In this case with a more closer look the oscillation starts at the mean value of 4.1% at time 0, decreases to a minimum of 3.5%, then increases again to a maximum of 5% to then decrease to the mean value of 4.1 % at recorded time 1 second. Thus a full cycle has been captured for this (the most extreme case), furthermore for other cases the oscillations occur in smaller time intervals. Even if a 1 second interval is sufficient to capture a full oscillation of the system, either longer sampling times should be taken or many repeats should be done to make sure it is representative of the bubble dissolution system.

4.1.3 Bubble size distribution and probability density function

In order to establish a comparison on the shape the bubble size distributions between the different impellers sections, it was necessary to normalize the number distributions to a probability density function (pdf) for all the bubble diameter intervals. The Weibull pdf is chosen as it is defined positive only for positive values. This distribution includes the exponential and the Rayleigh distributions as special cases (Kotz et al., 2000), and with variations on their shape parameter *"c"* and scale parameter *"d"* the distribution form can adapt to the data recollected on the current research better than for example a normal or quadratic distribution. The Weibull pdf for a variable *"x"* ($f_{Weibull}$) is defined as:

$$f_{Weibull}(x|c,d) = \frac{d}{c}\left(\frac{x}{c}\right)^{d-1} e^{-\left(\frac{x}{c}\right)^{d}} \quad (Eq.6)$$

In Fig. 8.a an overlapping of the bubble probability density data for air, with the mean bubble diameter oscillating between 3.7 and 4.5 mm. Even if the distributions present a bi-modal behavior for the air case, in contrast with the single modal behavior of the CO_2 case; the air data distribution presents no variations in term of impeller position. No clear tendency can be observed from the probability density data shape in terms of the impeller position. On the contrary for CO_2 in Fig. 8.b a clear effect on the bubble Weibull pdf is seen as the distribution tends to shift towards smaller bubble diameters intervals as the impeller number increases i.e. higher up in the bubble reactor, with high coefficient of regression values R^2 between 0.8683 and 0.6391.

Finally, the Weibull distribution is widely used in so-called survival analysis (Pham, 2006), which attempts to answer questions such as: what is the proportion of a population which will survive past a certain time? In this context, the authors saw a natural link on how a population of bubbles in a bubble swarm evolves due to dissolution, thus the number of bubbles and their size decrease seem to fit this line of thought. Since a distribution type must be selected, the Weibull distribution is chosen for its versatile characteristics listed above. Nevertheless, perhaps the use of other distributions could also be suitable.

The parameters of each fit for CO_2 with their respective 95% confidence intervals are presented in Table 1. The Weibull pdf represents a suitable approximation as the variations on the 95% confidence intervals parameters is minor < 5%.

Although the air bubble size distributions seem bi-modal in Fig. 8, it is important to notice that the error ranges of standard deviation for bubble sizes < 3 mm are actually quite large in comparison to the number of bubbles in theses ranges, being > 40% and in some cases >80% in comparison with the number of bubbles located in those smaller size intervals. Due to large errors in this area, and thus to a fair fitting of a mono-modal Weibull distribution based on 95% confidence intervals for the Weibull parameters, the extra peak in these measurements is due experimental errors and not due an inherit bi-modal behavior of the air bubble system. These errors are most likely caused by highly non-spherical bubbles and depth of focus errors, which may be minimized with the use of a second camera for simultaneous recording in a perpendicular plane.

4.1.4 Comparison with earlier work

Finally, the main goal was to compare the present experimental results of bubble swarm dissolution while mixing the fluid with previous simulations and single bubble rise dissolution for CO_2. The authors earlier (Legendre and Zevenhoven, 2016) presented a Comsol one-way coupling method in a frozen rotor simulation of a reactor of similar characteristics and dimensions (4 sections, 50 cm, with centered pitched blade impellers rotating at 100 rpm), with bubbles of initial 5 mm diameter; these simulations were performed prior the building of the reactor. Results presented can aid to improve current efforts on bubble column simulations.

Fig. 9 shows a graphical representation of current experimental results for bubble swarms in a stirred reactor (colored in red), with earlier single bubble rising experiments (discrete points). Added are also numerical estimations on the dissolution of single bubbles on a 1D model and CFD Comsol simulations for a few bubbles (Legendre and Zevenhoven, 2016, 2017).

Experimental results on the dissolution of bubble swarms (≈120 bubbles) in terms of bubble Sauter diameter present an almost exact match with the experimental dissolution of a single rising bubble and the numerical estimation for one bubble according to Fig. 9. This trend changes for the last impeller N°4 (height 168 cm) as the rate of dissolution decreases, only this point giving perfect agreement with CFD simulations of bubble swarms. It seems that the CFD model overestimates the bubble average diameter for the first three (lowest) impeller sections. Due to the concavity of the bubble swarm experimental results in Fig. 9, it can be appreciated that the dissolution rate of the mean bubble diameter decreases as the bubble size decreases, i.e. bigger bubbles dissolve faster than smaller bubbles.

4.2 Effect of impeller rotation speed

In order to study the effect of the rotation on the dissolution of the bubbles, images from experiments with a maximum rotation speed of 200 rpm were recorded. In Fig. 10 it can be observed how there is a small decrement of the bubble mean diameter of 0.06 mm when changing from 100 rpm to 200 rpm for impeller N°2, in contrast with larger variation for impeller N°3 of 0.16 mm from 0 rpm to 100 rpm - see Fig. 11. Rotational speeds >100 rpm do seem less effective than speeds <100 rpm.

However, the bigger change is in the shape of the distribution as it can be observed how the bubble size distribution peak increases as the rotational speed increases in both cases.

5 Conclusions

Bubble swarm dissolution (58-140 bubbles) of CO_2 and air in water, in a bubble reactor was experimentally studied using high speed camera recording and image processing with a void area fraction <6.5%. The pH was monitored so the concentration of the solution <5% saturation is maintained during all experiments. Results show a distinction of CO_2 dissolving bubbles vs. air non-dissolving bubbles. Comparison with previous simulations shows a fair agreement with the experimental data. CFD one-way coupling bubble swarm simulations slightly overestimate the bubble dissolution diameter for bigger bubbles (lower column sections), but the accuracy of the results presents a good agreement for highest level impeller of the bubble reactor (upper section). This suggest that bigger bubbles since they have a bigger influence on the surrounding fluid than smaller ones are the cause of this overestimation, therefore two-way coupling simulations (where the influence of bubbles in the fluid is present) could narrow the gap between experimental and numerical results - this is part of ongoing work.

Commonly in the area of bubble reactors, a single value for a bubble diameter is used for design and construction. Even if the dissolution of a single bubble can describe the behavior of the mean diameter of a dissolving bubble swarm, since the width of the bubble size distribution cannot be inferred from a single bubble, perhaps the use of this mean diameter as design parameter is not sufficient to reflect the complex reality of bubble swarm dissolution. It is recommended to define not only the bubble mean, but also the width and shape of the bubble size distribution as design factors. As shown, the width of the bubble distributions reduces as the bubbles dissolves from bubbles with ranges 0-8 mm in the first, lowest section to bubbles of 0-3.5 mm in the fourth and highest section. Thus, the dissolution of bubble swarms in a bubble reactor must be studied not only in terms of the bubble mean diameter but also in terms of the width and shape of the distribution.

In terms of rotational speed, for the current case an increase of rotational speed from 0 to 100 rpm is more significant (approx. 10%) in terms of bubble dissolution than an increase from 100 to 200 rpm (approx. 3%). This leads to the result than an increase on rotational speed indeed enhances the bubble swarm dissolution but as the rotational speed increases this enhancement becomes less substantial. In industrial applications, this could translate to energy saving if a sufficient rotational speed is used for a certain reactor configuration.

Nevertheless, this information may not be sufficient to draw general conclusions on the effectiveness of higher or lower rotating speeds in CO_2 swarm dissolution, since several improvements can be made to the experimental configuration presented in the current paper. Perhaps as recommendation for future work, variations on impeller shapes, further variations on rotating speeds, or different initial bubble sizes are studied.

Finally, some of the more relevant uncertainties of the experiments can be pointed out. One weakness of the current experimental set up is that a second camera for simultaneous recording in the perpendicular plane of the bubble tower was not available. This could verify if the bubbly flow is actually steady in the perpendicular plane of recordings at all times. An important recommendation for future research is to measure the agitation and flow pattern produced by the impeller. This could clarify how the sideways movement of the flow and the unsteadiness of the flow affect the bubble motion, and to which extent affect the dissolution in terms of vertical or radial flow characteristics and bubble residence time. Also, the correction of the distortions due the curvature of the vessel was limited to one plane, causing errors on

corrections on the images and therefore large standard deviations values (in some cases > 25%) in the bubble diameters measured.

Acknowledgements

This work was funded by the Tekes / Aalto University TUTL project X2PCC (2016-2017) and (for DL) Finland's Graduate School for Chemical Engineering (2016-2017). Alf Hermanson of ÅA T&FE is acknowledged for help with the bubble column and video recording equipment. Dr. Ari Kankkunen of Aalto University is acknowledged for discussions and support with image analysis theory.

References

Azzopardi, B.J. (2011). Sauter mean diameter. In: Thermopedia, A-to-Z Guide to Thermodynamics, Heat and Mass Transfer, and Fluids Engineering, (Begellhouse), doi: 10.1615/AtoZ.s.sauter_mean_diameter. Accessed 2018-07-26.

Besagni, G., and Inzoli, F. (2016). Comprehensive experimental investigation of counter-current bubble column hydrodynamics: Holdup, flow regime transition, bubble size distributions and local flow properties. Chem. Eng. Sci. *146*, 259–290.

Besagni, G., Brazzale, P., Fiocca, A., and Inzoli, F. (2016). Estimation of bubble size distributions and shapes in two-phase bubble column using image analysis and optical probes. Flow Meas. Instrum. *52*, 190–207.

Böhm, L., Kurita, T., Kimura, K., and Kraume, M. (2014). Rising behaviour of single bubbles in narrow rectangular channels in Newtonian and non-Newtonian liquids. Int. J. Multiph. Flow *65*, 11–23.

Cheremisinoff, N.P. (2000). Handbook of Chemical Processing Equipment (United States of America: Butterworth-Heinemann).

Colombet, D., Legendre, D., Cockx, A., Guiraud, P., Risso, F., Daniel, C., and Galinat, S. (2011). Experimental study of mass transfer in a dense bubble swarm. Chem. Eng. Sci. *66*, 3432–3440.

Colombet, D., Legendre, D., Risso, F., Cockx, A., and Guiraud, P. (2015). Dynamics and mass transfer of rising bubbles in a homogenous swarm at large gas volume fraction. J. Fluid Mech. *763*, 254–285.

Ferreira, A., Pereira, G., Teixeira, J.A., and Rocha, F. (2012). Statistical tool combined with image analysis to characterize hydrodynamics and mass transfer in a bubble column. Chem. Eng. J. *180*, 216–228.

Michon, G.P. (2000). Spheroids & Scalene Ellipsoids. http://www.numericana.com/answer/ellipsoid.htm. Accessed 2018-07-26.

Gong, X., Takagi, S., Huang, H., and Matsumoto, Y. (2007). A numerical study of mass transfer of ozone dissolution in bubble plumes with an Euler – Lagrange method. Chem. Eng. Sci. *62*, 1081–1093.

Honkanen, M., Saarenrinne, P., Stoor, T., and Niinimäki, J. (2005). Recognition of highly overlapping ellipse-like bubble images. Meas. Sci. Technol. *16*, 1760–1770.

Huang, Z., McClure, D.D., Barton, G.W., Fletcher, D.F., and Kavanagh, J.M. (2018). Assessment of the impact of bubble size modelling in CFD simulations of alternative bubble column configurations operating in the heterogeneous regime. Chem. Eng. Sci. *186*, 88–101.

Jakobsen, H.A. (2001). Phase distribution phenomena in two-phase bubble column reactors. Chem. Eng. Sci. *56*, 1049–1056.

Joshi, J.B. (2001). Computational flow modelling and design of bubble column reactors. Chem. Eng. Sci. *56*, 5893–5933.

Klamkin, M.S. (1971). Elementary Approximations to the Area of N-Dimensional Ellipsoids. Am. Math. Mon. *78*, 280–283.

Kotz, S., Balakrishnan, N., and Johnson, N.L. (2000). Continuos Multivariate Distributions. Volume 1: Models and Applications. (Canada: John Wiley & Sons, Inc.).

Laakkonen, M., Moilanen, P., Miettinen, T., Saari, K., Honkanen, M., Saarenrinne, P., and Aittamaa, J. (2005). Local bubble size distributions in agitated vessel comparison of three experimental techniques. Chem. Eng. Res. Des. *83*, 50–58.

Legendre, D., and Zevenhoven, R. (2016). A numerical Euler-Lagrange method for bubble tower CO_2 dissolution modeling. Chem. Eng. Res. Des. *111*, 49-62

Legendre, D., and Zevenhoven, R. (2017). Detailed experimental study on the dissolution of CO_2 and air bubbles rising in water. Chem. Eng. Sci. *158*, 552–560.

Martín, M., Galán, M. a., Cerro, R.L., and Montes, F.J. (2011). Shape oscillating bubbles: hydrodynamics and mass transfer - a review. Bubble Sci. Eng. Technol. *3*, 48–63.

Mattila, H.-P., and Zevenhoven, R. (2014). Design of a continuous process setup for precipitated calcium carbonate production from steel converter slag. ChemSusChem. *3*, 903–913.

Nock, W.J., Heaven, S., and Banks, C.J. (2016). Mass transfer and gas – liquid interface properties of single CO_2 bubbles rising in tap water. Chem. Eng. Sci. *140*, 171–178.

Pham, H. (Ed. . (2006). Springer Handbook of Engineering Stadistics (NJ 08854, USA: Springer-Verlag London Limited).

Said, A., Laukkanen, T., and Järvinen, M. (2016). Pilot-scale experimental work on carbon dioxide sequestration using steelmaking slag. Appl. Energy *177*, 602–611.

Wang, S., Zhang, K., Xu, S., and Yang, X. (2018). Assessment of a bubble-based bi-disperse drag model for the simulation of a bubbling fluidized bed with a binary mixture. Powder Technol. *338*, 280–288.

Zhang, C., Yuan, X., Luo, Y., and Yu, G. (2018). Prediction of species concentration distribution using a rigorous turbulent mass diffusivity model for bubble column reactor simulation part I: Application to chemisorption process of CO_2 into NaOH solution. Chem. Eng. Sci. *184*, 161–171.

Zhong, S., Zou, X., Zhang, Z., and Tian, H. (2016). A flexible image analysis method for measuring bubble parameters. Chem. Eng. Sci. *141*, 143–153.

FIGURES

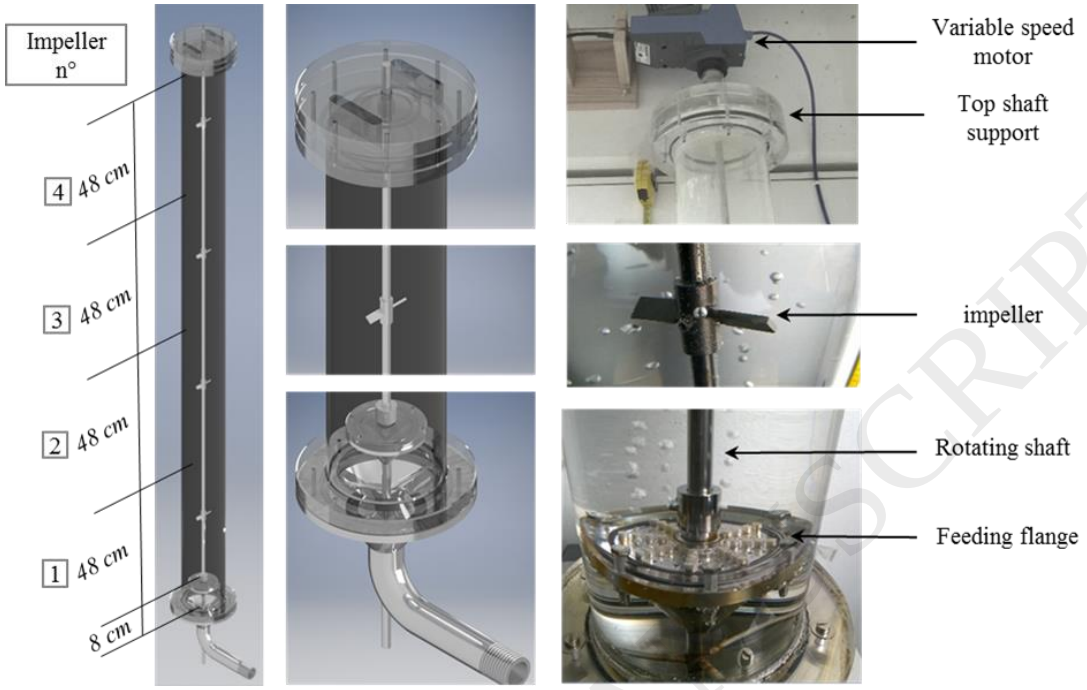

Figure 1. Bubble column used, with mixers locations and a close up of the gas distributor.

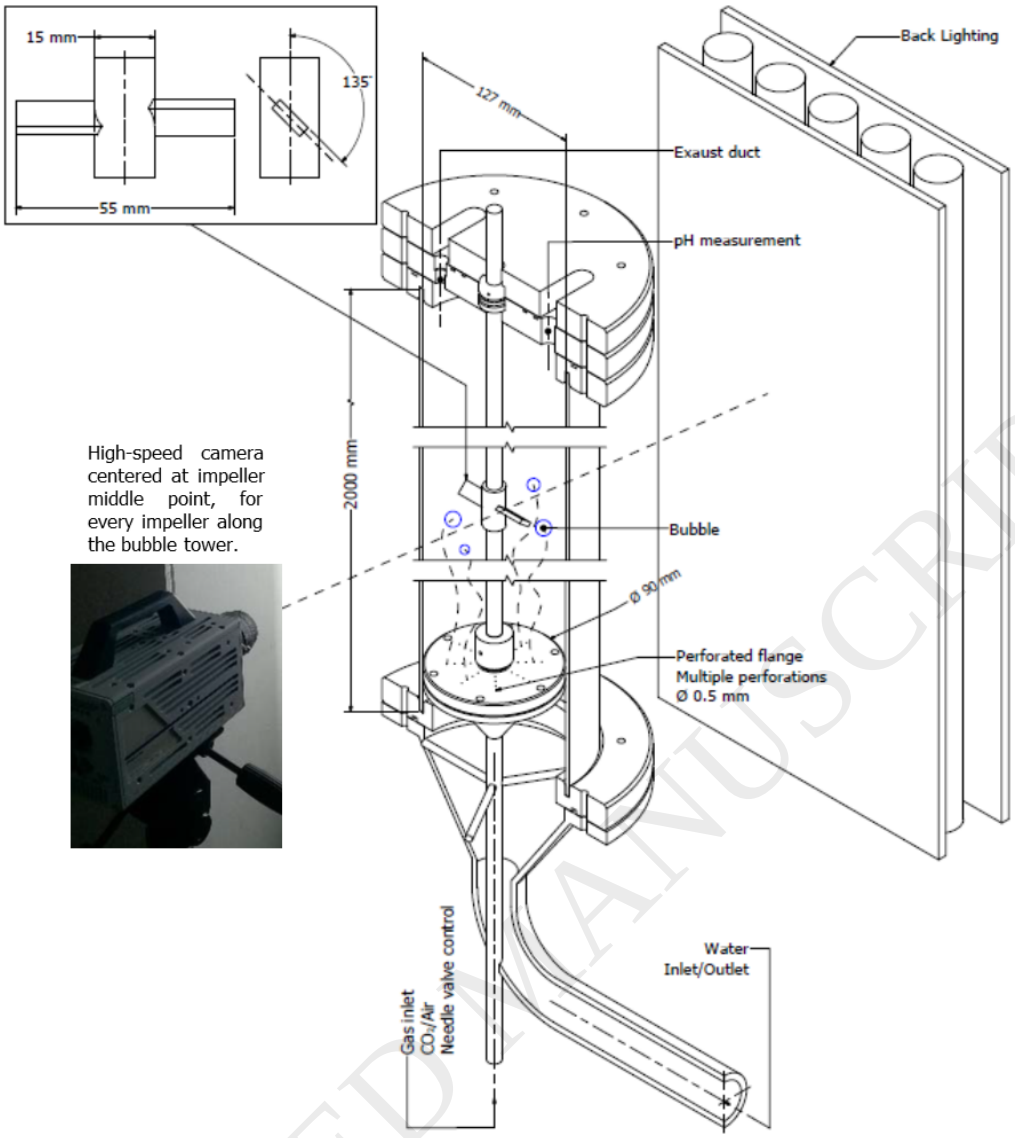

Figure 2. Semi-cross section of the bubble reactor with high-speed camera placement and back lighting.

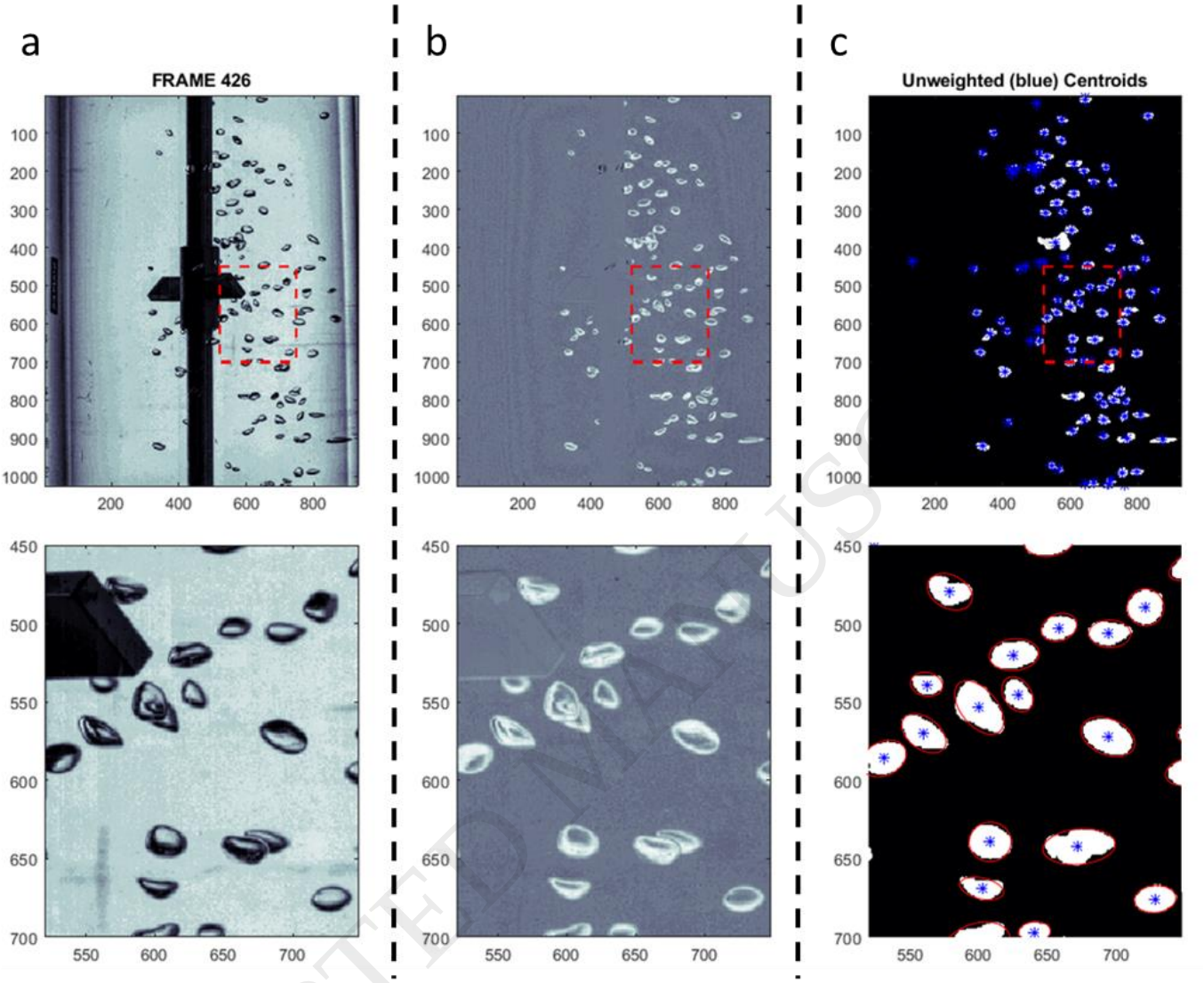

Figure 3. Size and shape estimation (a) high contrast image, (b) step i, (c) steps ii-vi.

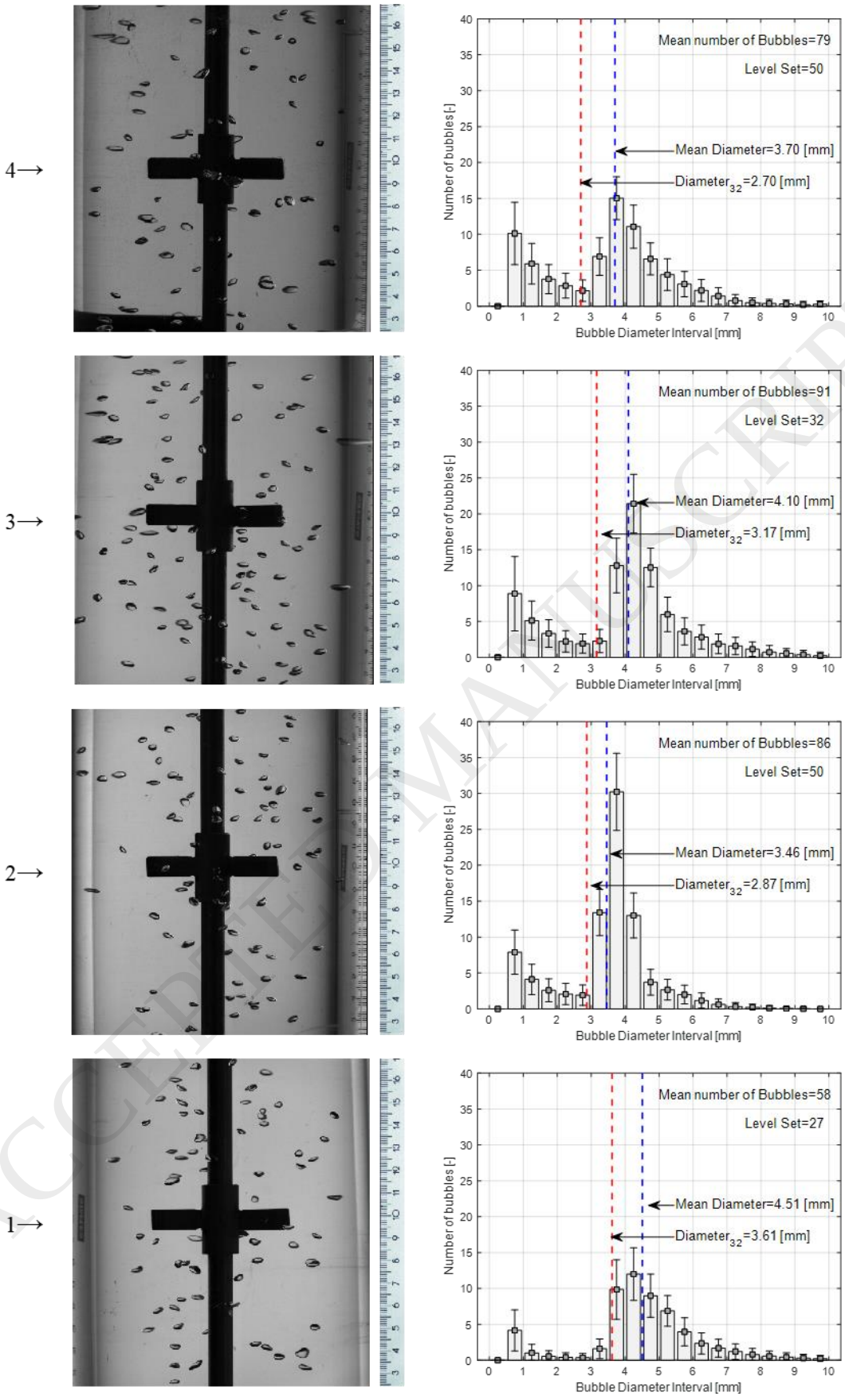

Figure 4. Air dissolution, impeller N° (left) and bubble size distribution (right)

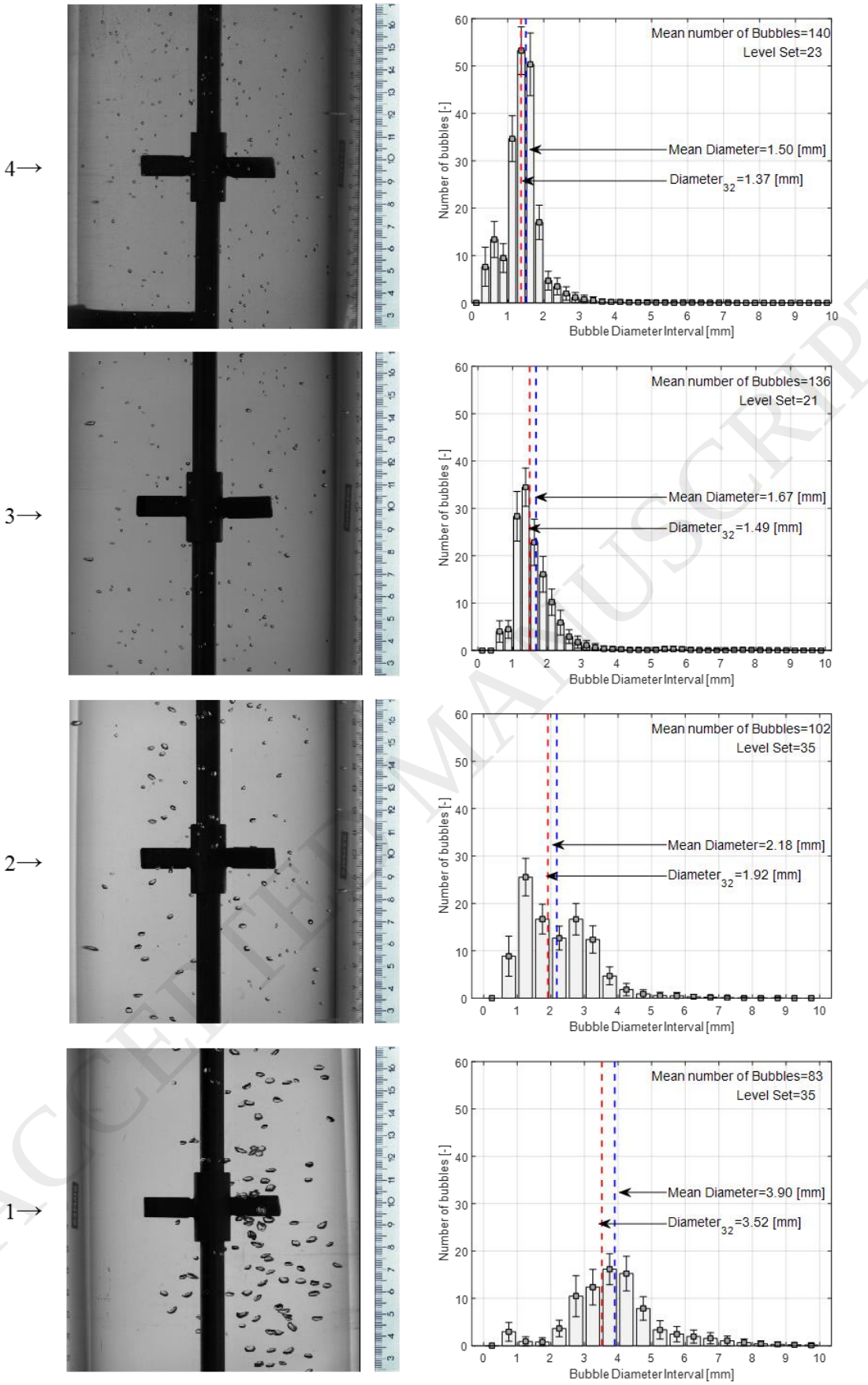

Figure 5. CO_2 dissolution, impeller N° (left) and bubble size distribution (right)

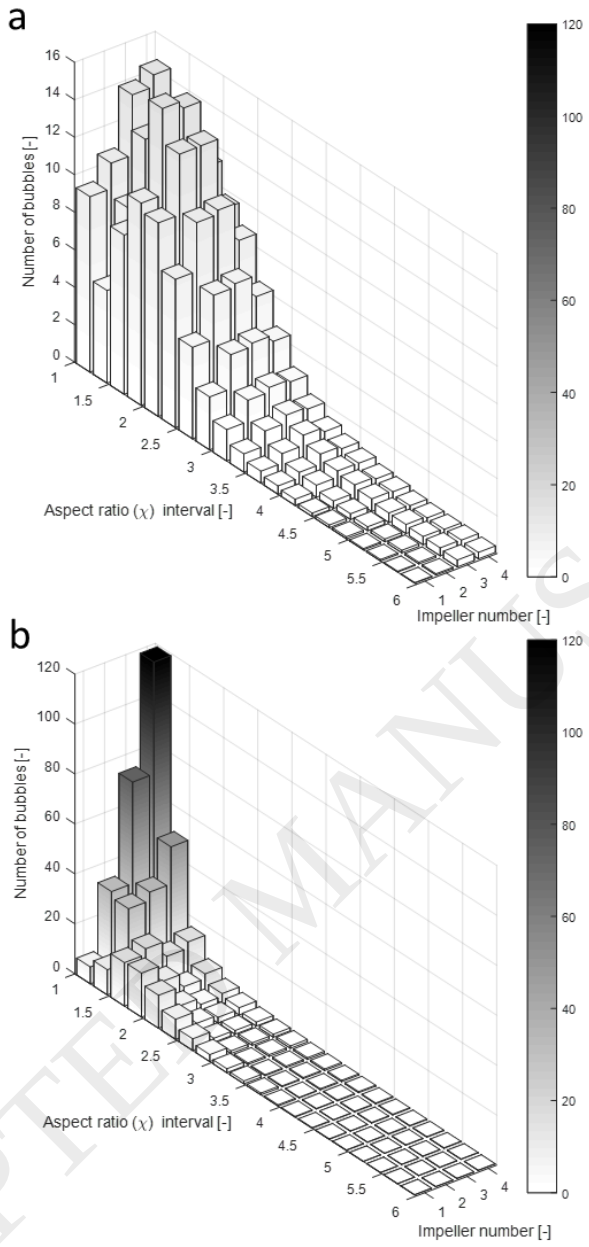

Figure 6. Bubble aspect ratio distribution by column (impeller) section.
(a) Air, (b) CO_2. Note the different axes.

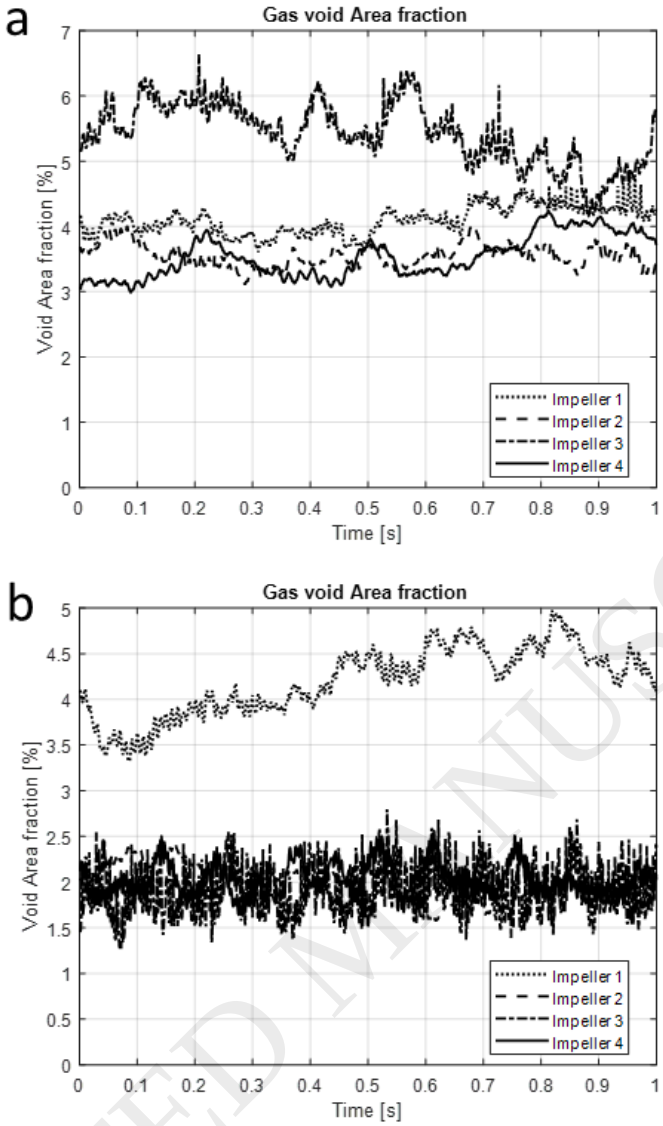

Figure 7. Gas area fraction. (a) Air, (b) CO_2.

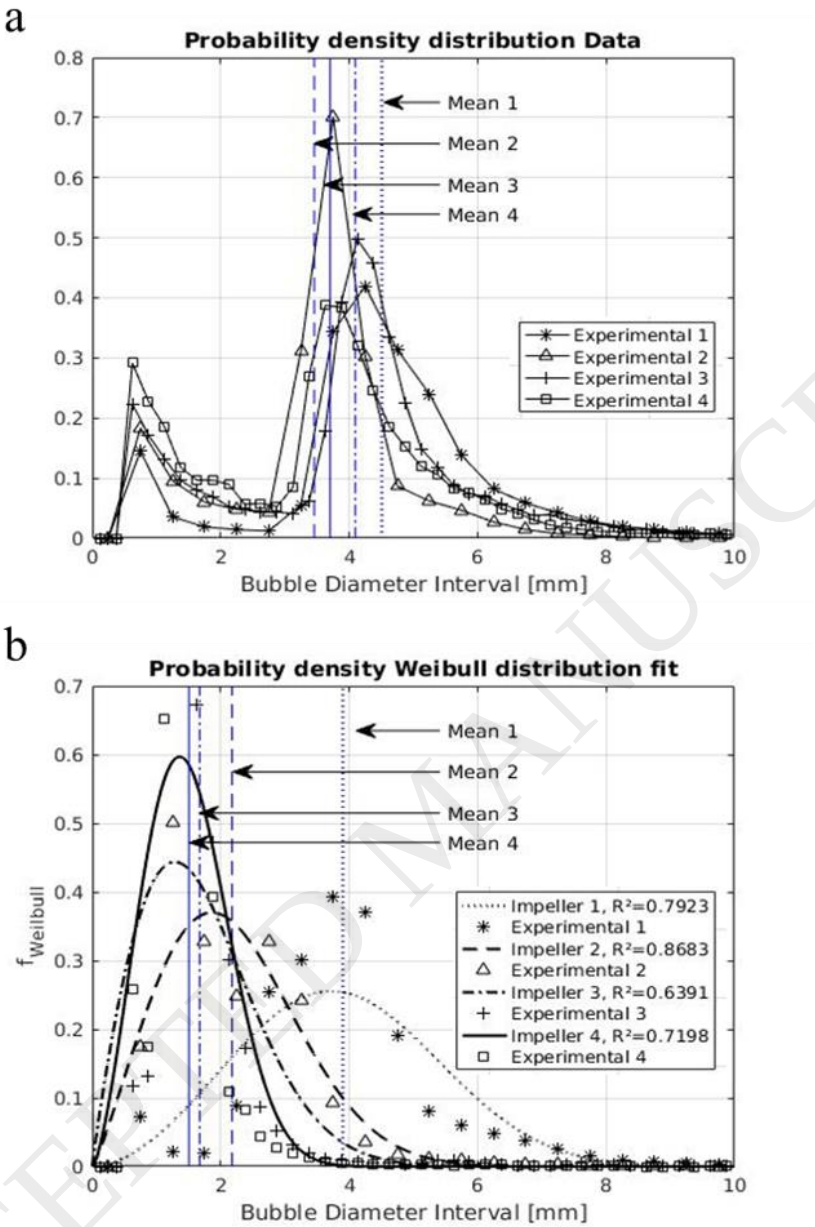

Figure 8. Probability density distribution for 4 column (impeller) sections. Including coefficient of determination R^2 for every distribution fit.

(a) Air Raw data, (b) CO_2 with Weibull distribution fit.

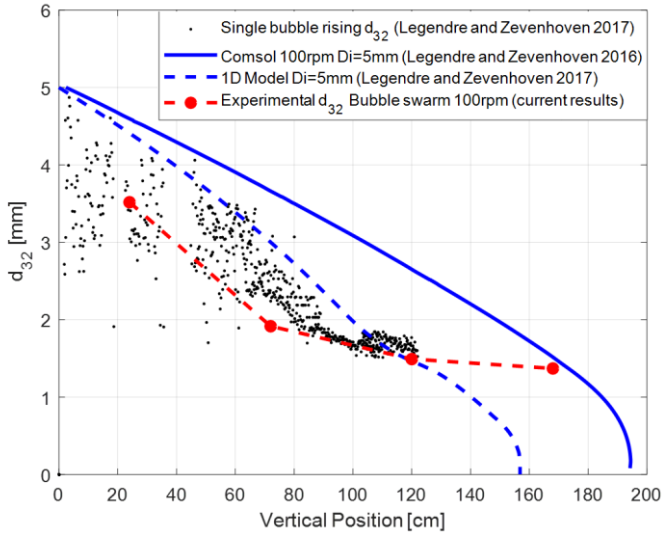

Figure 9. Bubble CO_2 dissolution, Sauter diameter reduction, earlier results (Legendre and Zevenhoven, 2016, 2017) versus current results (colored in red).

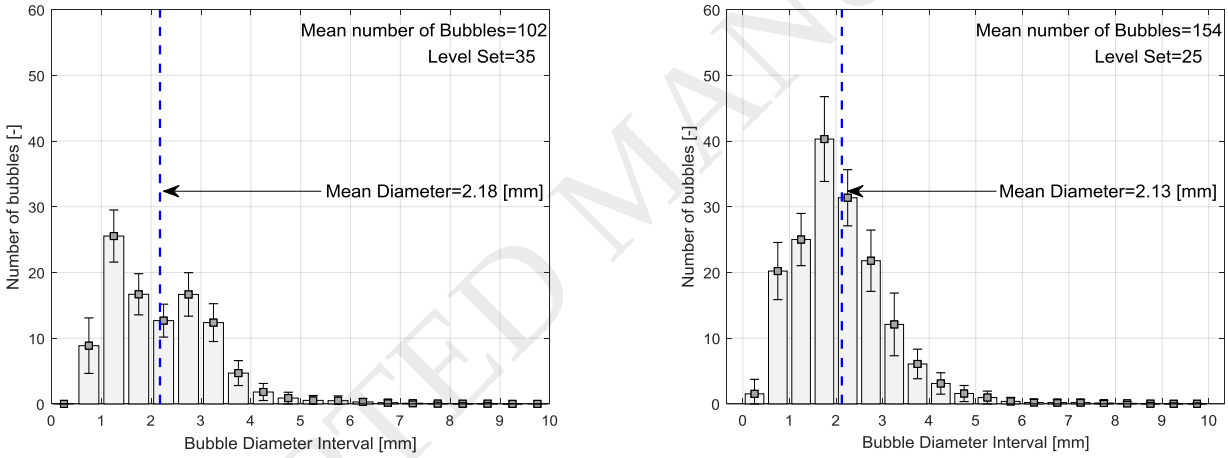

Figure 10. Bubble size distribution CO_2 2nd impeller. 100 rpm (left), 200 rpm (right).

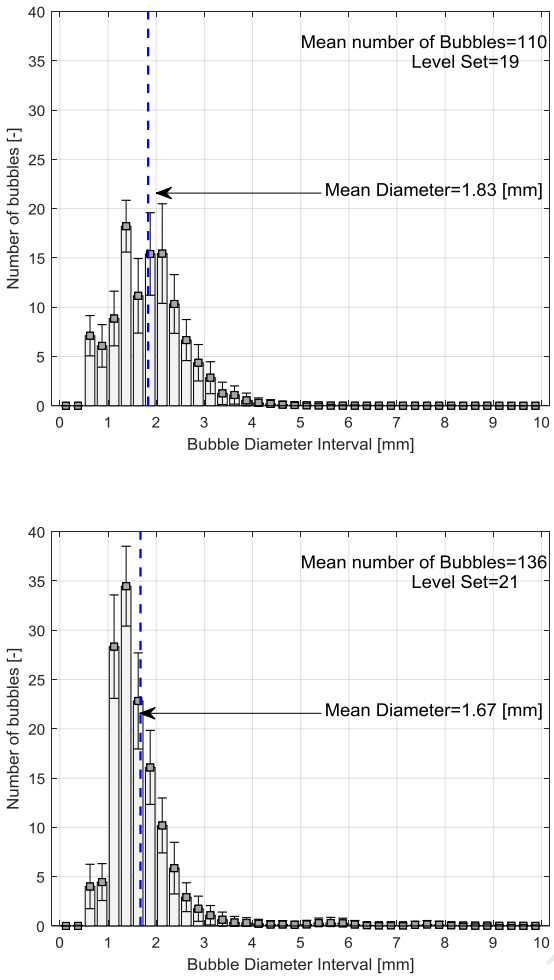

Figure 11. Bubble size distribution CO_2 3rd impeller. 0 rpm (left), 100 rpm (right).

Table 1. Weibull pdf parameters and confidence intervals for CO_2

Impeller n°	Scale parameter *"c"*	95% confidence intervals for *"c"*	Shape parameter *"d"*	95% confidence intervals for *"d"*
1	4.356	[4.345, 4.367]	2.812	[2.798, 2.826]
2	2.465	[2.457, 2.472]	2.185	[2.175, 2.195]
3	1.884	[1.878, 1.890]	1.920	[1.914, 1.926]
4	1.677	[1.673, 1.680]	2.471	[2.463, 2.479]